Chapter 21

Rotor Cage Fault Detection in Induction Motors by Motor Current Demodulation Analysis

Ivan Jaksch

Additional information is available at the end of the chapter

http://dx.doi.org/10.5772/47811

1. Introduction

Rotor cage faults as broken rotor bars, increased bars resistance and end-ring faults can be caused by thermal stresses, due to overload, overheating and thus mechanical stresses, magnetic stresses and dynamic stresses due to shaft torques. Environmental stresses as contamination or abrasion also contributes to the rotor cage faults. The rotor cage faults can also lead to the shaft vibration and thus bearing failures and air gap dynamic eccentricity.

Various rotor cage faults detection techniques for induction motors (IM) have been proposed during the last two decades. One of these is a widely used Motor Current Signature Analysis (MCSA) representing namely the direct spectral analysis of stator current (Thomson & Fenger, 2001; Jung et.al, 2006). MCSA can be combined with other methods as stray flux detection and a radial and axial vibration analysis. MCSA is still an open research topic, namely in the region of higher harmonics.

Strongly nonstationary working conditions as start-up current analysis require the application of methods generally called Joint Time Frequency Analysis (JTFA). These methods are Short Time Fourier Transform, Continuous Wavelet Transform (Cusido et.al, 2008; Riera-Guasp, 2008), Discrete Wavelet Transform (Kia et. al., 2009), Wigner Distribution (Blödt et al., 2008), etc. The fundamental of the wavelet analysis is the stator current decomposition into a determined number of detailed and approximation components and their pattern recognition. Wavelet analysis can be combined with other methods as a torsional vibration (Kia et. al., 2009).

The Vienna monitoring method –VMM (Kral et. al, 2008) is a rotor fault detection method based on instantaneous torque evaluation determined by voltage and current models. Other introduced methods for IM rotor fault diagnostics are multivariable monitoring (Concari et.al, 2008), artificial neural networks and neural network modeling (Su & Chong, 2007), fuzzy based approach (Zidani et. al., 2008), wavelet analysis together with hidden Markov

models (Lebaroud & Clerc, 2008), pendulous oscillation of rotor magnetic field (Mirafzal & Demerdash, 2005), vibration analysis (Dorrell et al., 1977) etc. A review of diagnostic techniques has been presented in several publications (Nandi et. al., 2005; Bellini et. al., 2008; Zhang et. al., 2011).

We can see that today it is not a problem to find rotor faults. What still remains a problem is to exactly and unambiguously determine fault indicator and its fault severity with a defined measurement uncertainty under changing motor parameters - various loads and inertia. Ideally the fault indicator should be independent on IM load. The examination of the various load influence on the fault indicator changes is very important especially in the industrial applications, where the keeping the same motor loads is often difficult. It has to be known what range of parameter changes are allowed for the keeping of the fault indicator constancy. As it is not known, at repeated measurements with different fault indicators, it is not clear, if the reason is due to the varied (deteriorating) IM faults or due to IM changing parameters. What is also important is the repeatability of the measurement with the same result. The third problem is a preferably simplicity and easy implementation of the methods for practical use in industry. Introduced new demodulation methods fulfill most of these requirements.

Dynamic rotor faults of IM, namely rotor broken bars and dynamic or combined eccentricity, cause a distortion of the rotor bars current distribution, and thus they cause periodical dynamic changes related to IM rotation frequency *fr* in the rotor magnetic field and consequently torque oscillation and therefore stator current modulation. The complex stator current analysis and experiments based on simultaneous amplitude and phase demodulation techniques proved that the stator current at rotor faults consists both of amplitude modulation (AM) and phase modulation (PM). AM and PM are combined into the Joint Amplitude Phase Modulation (JAPM). Amplitude and phase modulating currents are in certain relations, both in their amplitudes and mutual phases, dependent on motor load, inertia and also on IM working conditions.

Motor Current Demodulation Analysis - MCDA comes out from the fundamental principle which arises at dynamic rotor faults - IM stator current modulation. The basic idea of MCDA is to extract only those currents from the whole stator current which are directly induced and caused by rotor faults, and to investigate only these fault currents in the time and frequency domain. At health IM these currents do not exist, practically are near zero.

The demodulation is a process, how to gain back the information about the time course of modulating signal from modulated signal. Outputs of demodulation methods are, therefore, the direct time courses of modulating i.e. fault currents. The spectrum of a fault current does not contain any sideband components, fault frequencies are determined directly and only one spectral peak represents the fault indicator. The great advantage of MCDA is its easy use in industrial diagnostics.

Most of the present diagnostic methods, both for stationary and non-stationary (Joint Time-Frequency Analysis) IM working conditions, use full IM current analysis methods for rotor fault detection. Just MCDA proved the complexity of the IM current at dynamic rotor faults and therefore the dependence of fault indicators based on full IM current on IM

working conditions. It is mostly various IM loads which changes PM and great inertia or insufficient IM feeding which change an angle φ between AM and PM and therefore cause the dependence. These rotor fault indicators dependence cannot be removed.

2. The analysis of IM current and current signature at rotor faults

The widely used rotor fault detection technique - MCSA is presented in a large number of publications. This approach analyses whole IM stator current uses the spectral low and high slip pole frequency $2sf_1$ sidebands a_{APL}, a_{APH} around the supply frequency f_1 for broken bars detection (Bellini et. al., 2001). According to this theory, magnetic rotor asymmetry causes a backward rotating field and formation of a current component a_{APL} at the low sideband frequency f_1-f_{sp}. The consequent torque and speed oscillation cause the occurrence of a new component a_{APH} at the high sideband frequency f_1+f_{sp}. First, the only low sideband spectral magnitude was taken as a fault indicator for broken bars. Later a new diagnostic index was introduced as a sum of the two spectral sideband components a_{APL}+a_{APH}.

Presented theory of the spectral low a_{APL} and high a_{APH} sidebands origination and formation and broken bars detection is quite different from MCSA theory. The theory comes from general modulation principles and exactly determinates both sidebands origination including the equations for a_{APL}, a_{APH} computation.

An exact detailed analysis of the stator current content at broken bars from the view of the complex air-gap rotor electromagnetic field analysis representing simultaneous stator current AM and PM, their mutual relation and changes at different load and inertia moment, and their formation to the MCS a_{APL} and a_{APH} magnitudes has been missing so far.

2.1. Broken bars stator current modulation and its contribution to the MCS formation

Introduced theory and rotor fault analysis and diagnostics come from the basic principle when periodical changes in rotor magnetomotive force (MMF) cause the periodical changes of IM stator current amplitude and phase, and thus the stator current AM and PM.

Broken rotor bars, as an electric fault, cause the rotor asymmetry, the distortion of the rotor current distribution, rotor current pulsation and its amplitude modulation by the slip frequency f_{slip}. Rotor bars current amplitude changes are transformed to stator current on slip pole frequency f_{sp} and appears here as a stator current AM. This modulation can be interpreted as a primary modulation.

Rotor bars current amplitude changes cause the changes in force on coils moving in a magnetic field. The force can be obtained from the vector cross product of the current vector and the flux density vector $F_x = NI\, \upsilon\phi/\upsilon x$, where NI is MMF, ϕ is linked magnetic flux and x is the force direction. Subsequently, the total force on a current carrying rotor coils (bars), moving in a magnetic field, changes and electromagnetic torque oscillation appears. Torsion vibration also can appear. Oscillating torque causes periodical changes in the rotating phase angle and therefore the stator current PM. This modulation can be interpreted as a

subsequent or secondary modulation, so PM cannot originate without AM and JAPM always exists. The JAPM can be interpreted as a stator current modulation by a complex modulating vector which changes both its amplitude and phase. Angular speed oscillation as the derivation of phase oscillation also appears.

The frequency of periodical changes is a slip pole frequency f_{sp} (suffix$_{sp}$) which is independent on the number of motor poles

$$f_{sp} = pf_{slip} = psf_{sync} = ps2f_l / p = 2sf_l = 2f_l - f_r p \tag{1}$$

For better understanding of a real IM state, which comes in IM current at dynamic rotor faults and for the explanation of a_{APL} and a_{APH} origination and formation from AM and PM, the properties of AM and PM have to be firstly well known. So the basic properties of AM and PM will be firstly presented before the explanation of the real IM state - JAMP.

2.1.1. Amplitude modulation-AM

AM is clearly visible from the time course of an IM current amplitude which is not stable, but changes according to the modulating current amplitude. It can be clearly seen as the IM current time course envelope already from about 2% deep of modulation I_{spa}/I_l representing approximately 2 broken bars.

Spectrum of AM (suffix $_A$) is derived from the Euler formula $cos(\omega t)=½(exp(j\omega t)+exp(-j\omega t))$ expressing the decomposition of a harmonic signal into the pair of rotating vectors (phasors) -Fig.1. Phasors' amplitudes are the half of the original harmonic signal amplitude; one rotates positive direction, the other rotates negative direction.

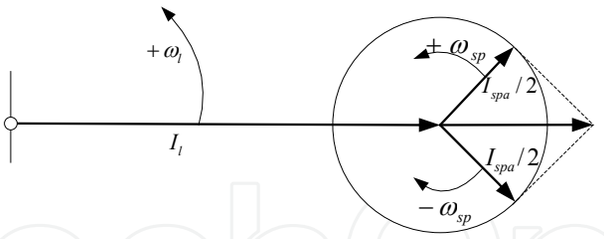

Figure 1. Vector representation of AM for broken bars

Spectra of modulated signals are always connected with two sidebands peaks around the carrier signal spectral peak. AM appears in the autospectrum of the modulated signal as three peaks: one at the carrier frequency with the magnitude equal to the amplitude of carrier signal and two sidebands spaced by modulating frequency from the carrier frequency each of them with the half amplitude of the modulating signal.

For broken bars there are two sideband components at low and high frequency $f_{L,H}$ and their low and high sidebands magnitudes a_{AL}, a_{AH} have the same size a_A which equals the half of the amplitude of the modulating current I_{spa}

$$f_{L,H} = f_l \pm f_{sp} \qquad a_A = a_{AL} = a_{AH} = I_{spa} / 2 \tag{2}$$

2.1.2. Phase modulation-PM

Unlike AM, PM is not observable from the stator current time course at so small modulation indexes to 0.15. PM can be visible as stator current time course compression and decompression from modulation indexes greater than 2, which are approximately 10 times higher than the usual modulation indexes at broken bars.

The spectrum of phase modulation (suffix $_P$) is dependent on the modulation index size. If the modulation index is greater than *1*, the PM spectrum consists of many side components, if it is lower than *0.4*, the spectrum contains only a few side components. The spectral magnitudes computation of phase-modulated signals requires the use of the Bessel functions J_i, $i=1, 2,..,M$ (Randall, 1987).

The real modulation indexes at rotor faults, expressed by I_{spp}, are very low about to max. *0.15* at large rotor faults and in this case the stator current autospectrum contains only two significant sideband components $J_1(I_{spp})$ with the same magnitudes $a_{PL,H} = a_P$ equal to the half of the I_{spp} multiplied by phase current amplitude I_l. (Bessel functions are not needed).

$$f_{L,H} = f_l \pm f_{sp} \qquad a_P = a_{PL} = a_{PH} = I_l I_{spp} / 2 \tag{3}$$

The result is that the autospectrum of PM current looks the same as the autospectrum of AM current. But the substantial difference is in the initial phases of sidebands magnitudes at $f_l - f_{sp}$ and $f_l + f_{sp}$ frequencies, Table 1., 2nd row, bold, and Fig.2. Spectral sideband magnitudes a_{PL}, a_{PH} increase both owing to I_{spp} and also owing to I_l, unlike at AM, see (2).

Component frequency	f_l-2f_{sp}	f_l-f_{sp}	f_l	f_l+f_{sp}	f_l+2f_{sp}
Initial phase	$\pi-2\phi$	$\boldsymbol{\pi/2-\varphi}$	*0*	$\boldsymbol{\pi/2+\varphi}$	$\pi+2\varphi$
Component amplitude	$J_2(I_{spp})$	$J_1(I_{spp})$	$J_0(I_{spp})$	$J_1(I_{spp})$	$J_2(I_{spp})$

Table 1. Frequencies and phases of the first 2 sidebands components of PM

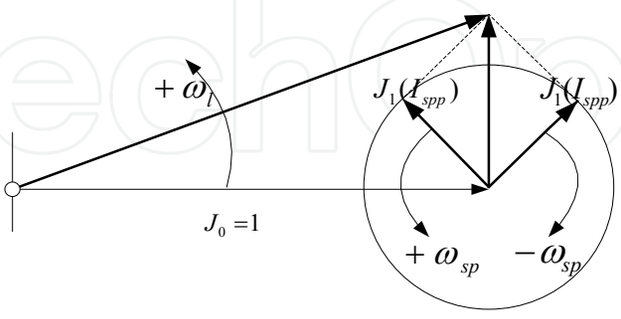

Figure 2. Vector representation of PM for broken bars

Table 1 and Fig.2 show that the initial phase of Bessel function J_1 is $\pi/2$ so the resulting vector of PM is perpendicular to the resulting vector of AM. The initial phase shift for the component at f_l+f_{sp} is the original phase shift $+\varphi$ of the modulating signal, the initial phase for the component at f_l+f_{sp} is $-\varphi$ (a highlight and bold in Table 1, middle row).

2.1.3. JAPM and MCS–the real motor state at broken bars

This type of modulation expresses exactly the real motor state at broken bars. Both AM and PM have the same frequencies and their amplitudes and phase shifts between them are in certain relations depending on IM load and inertia. Providing sinusoidal currents, the IM current of healthy motor $i_a=I_l \cos(\omega_l t)$ changes at rotor broken bars to

$$i_a = \left(I_l + I_{spa}\cos\omega_{sp}t\right)\cos(\omega_l t - I_{spp}\cos(\omega_{sp}t + \varphi)) \tag{4}$$

which contains both AM and PM. Amplitude modulating current $i_{AM} = I_{spa}\cos\omega_{sp}t$, phase modulating current $i_{PM} = -I_{spp}\cos(\omega_{sp}t + \varphi)$. The term I_{spa}/I_l represents the deep of modulation of AM and I_{spp} represents the modulation index of PM.

At low inertia and normal and stable working conditions the AM and PM currents have exactly opposite phases $\varphi_0=\pi$, $\varphi=0$. This results from the IM torque-speed characteristic, where torque changes induced by MMF changes induce opposite changes in speed.

The necessary condition for both MCS low a_{APL} and high a_{APH} autospectral magnitudes equality is the mutual perpendicularity of vectors forming AM and PM, Fig.1, 2 and Table 1. It occurs only in the case of exactly coincident or exactly opposite phases of AM and PM.

Since the necessary condition is fulfilled, the resulting low a_{APL} and high a_{APH} autospectral sideband magnitudes of JAPM have the same size given by (5).

$$a_{APL} = a_{APH} = \sqrt{a_A^2 + a_P^2} \tag{5}$$

Unfortunately from sideband magnitudes a_{APL}, a_{APH}, which are the results of the widely used MCS, the contribution of AM and PM cannot be found out. Only demodulation techniques can find them.

Increasing IM load causes the increase of IM current I_l. Previous investigations and experiments (Jaksch & Zalud, 2010) proved also an increasing oscillation of rotor magnetic field at f_{sp} with increasing load which means the increase of I_{spp}. It means consequently the increase of a_{APL}, a_{APH} according to (3) at the same rotor fault size (dash line in Fig.3). The result is that PM is the main reason of a_{APL}, a_{APH} dependence on IM load.

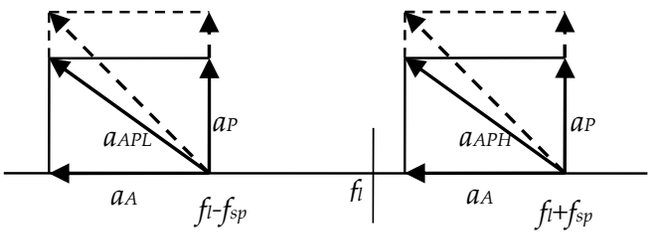

Figure 3. The formation of MCS a_{APL}, a_{APH} at broken bars from JAPM, φ=0, increasing motor load means the increase of PM –dash line.

Generally the inertia influences dynamic behavior of systems. Great inertia causes the increase of the mechanical time constant of the motor rotating system and therefore the delay $-\varphi$ (φ <0) of PM behind AM on f_{sp}. IM current spectrum symmetry and a_{APL}, a_{APH} equality disappears. The initial phase shift for the positive component at $f_l + f_{sp}$ frequency is $+\varphi$, see bold in Table I, and therefore a_{APH} decreases, the initial phases shift for the negative component at $f_l - f_{sp}$ is $-\varphi$ and therefore the a_{APL} increases -Fig.4. The angle between AM and PM modulation vectors is not $\pi/2$, (5) is not valid and the resulting a_{APL}, a_{APH}, are the vector sum of AM and PM rotating vectors.

Spectral magnitudes $a_{APL,H}$ of MCS can be computed according to the modified cosine low.

$$a_{APL,H} = \sqrt{a_A^2 + a_P^2 - 2a_A a_P \sin(\mp\varphi)} \tag{6}$$

For φ=0 this general equation for MCS computation, equation (6) changes to equation (5).

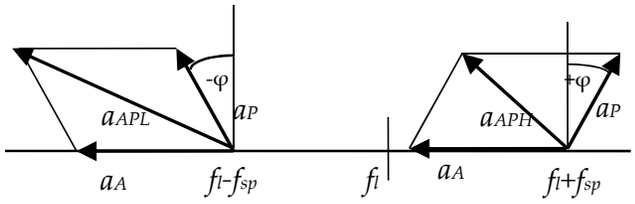

Figure 4. The formation of MCS a_{APL}, a_{APH} at broken bars from JAPM at great inertia, φ= -π/6

In the case of the extremely large inertia the shift between AM and PM is almost φ= -π/2. The result is that only the low spectral sideband component appears, see (6), with and the right sideband component is almost zero. The result is only theoretical.

The same comes in the case of overloaded and insufficiently fed IM by the voltage substantially lower than nominal AC voltage, which can be named as "abnormal working condition", when PM cannot follow AM and φ<0. In all other cases of normal IM working condition a_{APL}, a_{APH} should be the same size, in the range of possible Digital signal processing (DSP) errors.

Based on the JAMP the phenomena which appear in dynamic motor modes like start-up or breaking and their formation to a_{APL} and a_{APH} can be explained.

2.2. Dynamic eccentricity IM current modulation

The rotor cage faults can also lead to the mechanical stresses, shaft torques, bearing failures and therefore air gap dynamic eccentricity (Joksimovic, 2005; Drif & Cardoso, 2008). So the dynamic eccentricity, as a mechanical fault, closely relates to the rotor cage faults. Dynamic eccentricity is the condition of the unequal air gap between the stator and rotor caused namely by loose or bent rotor, worn bearing etc. IM current analysis is the base method, but the vibration as the cause of unbalance and the torsional vibration as the cause of the torque oscillation can be also performed as supporting method, but IM current related detection

methods in most cases give very good results. Relative dynamic eccentricity is defined as the ratio of the difference between the rotor and the stator center to the difference between the stator and the rotor radius. The values of dynamic eccentricity are 0-1 or 0-100%.

Dynamic or combined eccentricity and subsequently the air gap alternation changes the rotor electromagnetic field ones per IM revolution, so the modulating frequency is the rotation frequency f_r (suffix $_r$). IM spectrum contains two sidebands around f_l.

$$f_{L,H} = f_l \pm f_r \tag{7}$$

Spectrum of demodulated current contains peaks on direct frequencies f_r. The air gap changes do not contain stepping changes and the change usually pass subsequently during one revolution, so modulating current is often almost harmonic and contains only small higher harmonics, unlike modulating current for broken bars.

Providing sinusoidal currents, the motor current of healthy motor $i_a=I_l \cos(\omega_l t)$ changes at rotor dynamic eccentricity to

$$i_a = \left(I_l + I_{ra}\cos\omega_r t\right)\cos(\omega_l t - I_{rp}\cos(\omega_r t)) \tag{8}$$

which contains both AM and PM.

2.3. The influence of the time varying load

Until now the modulations caused by the internal IM rotor faults were solved providing IM different, but constant load when MCDA spectrum contains two significant peaks on f_{sp} and f_r , see Fig.6. In the case of the external periodical harmonic time varying load, which varies with the frequency $f_{load} < f_l$, both additional AM and PM of IM current arise on the f_{load} frequency. It can come e.g. in the case when IM drives machines with various machine cycles e.g. textile machines, machine tools etc. (In the case of the speed reducing devices as gearbox transmissions, the gear-ratio has to be counted for f_{load} determination).

In the IM full current spectrum - MCS two additional spectral sidebands peaks appear on frequencies $f_l \pm f_{load}$. In MCDA spectrum the time varying load appears as a one spectral peak on f_{load} with the magnitude proportional to a load torque difference which can be expressed as an I_{load}. So together 3 significant spectral peaks on f_{sp}, f_r and f_{load} appear in MCDA spectrum of IM with rotor faults. The AM can be also observed in the time course of IM current as the stator current envelope or in the time course of amplitude demodulated current.

If f_{load} equals exactly f_{sp} or f_r the rotor faults diagnostics is not correct because the resulting spectral magnitudes are the vector sum of the corresponding modulating amplitudes. The situation when $f_{load}=f_r$ can come when IM directly drives a machine with uneven load during one revolution e.g. a cam mounted on the main shaft. But practically it is a minimal probability that f_{load} equals f_{sp} or f_r. The minimal difference between f_{load} and f_{sp} or f_r is at Hanning window approximately 4 discrete step Δf. Usually used acquisition time is $T= 4s$, $\Delta f=1/T= 0.25$ Hz, so a minimal difference between external f_{load} and rotor faults frequencies f_{sp},

f_r is roughly 1Hz for the rotor fault diagnostic not influenced by the time varying load. The f_{sp} computation from f_r (1), enables the differentiation and subsequently the omission of an additional disturbing spectral peak on f_{load}.

Small external time varying load can be also caused by the fault of IM driven devices as a gearbox. In MCDA spectrum another peak appears and by the allocation of this peak frequency to the gearbox relevant mechanism frequency, the device fault can be identified.

3. Demodulation methods for rotor faults

Generally, the demodulation methods extract the original AM and PM signals using special computation methods. Now the demodulated signals are original modulating signals.

Demodulation methods can be used without precarious presumption whether the signal is modulated or not and in the case of no modulation, the demodulation results are zeros (PM) or constants (AM) and by removing DC also zeros.

For the determination of the modulated signal instantaneous amplitude and phase, a complex analytical signal has to be defined and created. An analytical complex signal created by mathematical formula is the base for the demodulation analysis. The most used methods are Hilbert transform, Hilbert-Huang transform or quadrate mixing. For 3-phase motors rotor faults a new method based on the space transform was developed.

The rotor fault amplitude demodulation extracts the original AM current. The AM current appears in stator current as an envelope of this current -Fig.5. Therefore the amplitude demodulation is known as an envelope analysis (Jaksch, 2003). It is the base for dynamic rotor fault diagnostics.

At broken bars, phase demodulation extracts PM current I_{spp} [A] which, as an argument of harmonic function (4), really represents the phase angle ripple or phase swinging [rad]. The phase demodulation gives the time course of the instantaneous swinging angle or instantaneous angular speed and represents a huge tool for the research of the rotor magnetic field oscillation, sensor-less angular speed, speed variation or other irregularities.

The demodulation analysis should be used for band pass filtered signals with the center in a carrier frequency and span corresponding to the maximal modulating frequency. Spectrum of demodulated current outside this bandwidth is shifted by a carrier frequency towards to the low frequencies. For IM rotor faults the carrier frequency is usually a supply frequency f_1 and the maximal modulating frequency is f_r, so the basic bandwidth $0\text{-}2f_1$ is suitable. In the case when analog bandwidth $0\text{-}2f_1$ cannot be kept it is possible to use higher bandwidths, but Shannon sampling theorem has to be strictly kept and demodulated spectrum must be evaluated only in the range of $0\text{-}f_1$ because for higher frequencies is not valid.

Higher order harmonics of supply current and also modulating broken bar current should appear as sideband components at frequencies $f_{k,l} = kf_1 \pm 2lsf_1$, $k=3,5,7$, $l= 1,2,3$ where k represents the index for stator current harmonics and l represents the index for broken bar

sideband current harmonics. Because of the interaction of time harmonics with a space harmonics, a saturation related permeance harmonics together with phase shifts of AM and PM means that some sidebands harmonics are suppressed and only certain ones can appear, so the above introduced formula is not generally valid.

Demodulation in the region of higher *k*-harmonics of the supply frequency requires the shift of the supply carrier frequency kf_1 to zero before the demodulation. It means the spectral frequency resolution Δf increasing which is often called Band Selectable Fourier Analysis (BSFA) or Zoom. Dynamic signal analyzers are equipped with this function (zoom mode) and a maximal Δf = 1mHz. However, this analysis has a little practical sense, because of above mentioned problems with higher order harmonics. In addition the modulating currents there usually have smaller amplitudes.

3.1. The demodulation using Hilbert transformation

The Hilbert transform (Bendat, 1989) is a well-known tool which enables to create an artificial complex signal $H(t)= x(t)+jy(t)$, called analytical signal, from a real input signal $x(t)$. The real part $x(t)$ of the analytical signal $H(t)$ is the original signal – stator current, the imaginary part $jy(t)$ represents the Hilbert transform of a real part $x(t)$. The absolute value $magH(t)$ representing amplitude demodulation and the phase $\beta(t)$ representing phase demodulation can be computed according to (9), (10).

$$magH(t) = \sqrt{x^2(t) + y^2}(t) \tag{9}$$

$$\beta(t) = \arctan(y(t) / x(t)) \quad in < -\pi, \pi > \tag{10}$$

The amplitude demodulation computation is quite easy and can be used for continual monitoring and diagnostics in real time.

Phase determination $\beta(t)$ [rad] from a complex number position holds only in the range $<-\pi, \pi>$ and if the phase overlaps these limits, it is necessary to unwrap it and moreover to remove the phase trend component which increases by2π every revolution with the increase of the common phase carrier signal (Randall, 1987). The computation of phase demodulation is a little difficult comparing to amplitude demodulation, but generally there is usually no problem with the phase demodulation computation.

3.2. The demodulation using space transformation

The space (Park) transform, based on the physical motor model, is used primarily for the motor vector control. A three phase i_a, i_b, i_c, $i_a(t)=I_1 \cos(\omega t)$ system is expressed in one space current vector $\boldsymbol{i}= K_s (i_a + a\, i_b + a^2 i_c)$, $a= e^{j2\pi/3}$ projected to the complex *d-q* plane (11).

From the 3 possible choices of K_s: $K_s = 1$ - amplitude invariance, $K_s = sqrt(2/3)$- power invariance, K_s=2/3 is used. In this case the additional recomputation coefficient between phase currents and transformed currents does not have to be used.

$$i_d(t) = (2/3)i_a(t) - (1/3)i_b(t) - (1/3)i_c(t)$$
$$i_q(t) = (\sqrt{3}/3)i_b(t) - (\sqrt{3}/3)i_c(t) \quad (11)$$

Space transform was firstly also used for the demodulation (Jaksch, 2003). From the viewpoint of the means necessary for the demodulation process, space vector $P(t)=i_d(t)+ji_q(t)$ represents a complex analytical signal computed from three three currents i_a, i_b, i_c similarly like the Hilbert transform creates the artificial complex signal $H(t)$ from one phase current.

The absolute value $magP(t)=sqrt(i_d^2(t)+i_q^2(t))$ forms the amplitude demodulation, $\beta(t) = arctan\ (i_q(t)/\ i_d\ (t))$ forms the phase demodulation.

3.3. The comparison of both demodulation methods

The space transform requires 3 currents measurement, but only simple computation (11) and no other transformation for the complex analytical signal determination. On the contrary Hilbert transform needs only one current measurement, but $jy(t)$ computation.

The space transform creates the analytical signal from 3 currents. In order to obtain the same sizes of fault indicators as from Hilbert transform, (11), using K_s=2/3 must be kept.

Small differences between Hilbert and space transforms can occur in the following cases:

- The violation of the exact phase shift $a=e^{j2\pi/3}$ between IM phase currents (space transform supposes exact shift 2π/3).
- Power feeding voltage unbalance or great stator fault, which can cause greater IM currents unbalance.

The maximum error should not be greater than in the range of several percent. The experiment showed - see Table II., Table III, I_{spaH}, I_{spaP} that the differences are up to 5 %.

Amplitude demodulation can be implemented also by the other techniques resulting also from the three phase IM feeding system as an apparent power magnitude or a squared stator current space vector magnitude. However these methods are more complicated than the space transformation method and in addition the results of these methods are in units and dimensions which are not comparable with the Hilbert transform results.

4. Simulation results

Various simulations have been performed. The main aim of the simulation was the verification of (5), (6) for the IM current MCS - a_{APL}, a_{APH} computation, namely the influence of angle φ on the sizes of a_{APL}, a_{APH}. The verification of the equality of MCDA fault indicators (lower window in Fig. 5) with input data values I_{spa}, I_{ra} also has been performed.

As it was previously derived in the section 2, the IM current of healthy motor $i_a=I_l\ cos(\omega_l t)$ changes at dynamic rotor faults - rotor broken bars and dynamic eccentricity to

$$i_a = \left(I_l + I_{spa}\cos\omega_{sp}t + I_{ra}\cos\omega_r t\right)\cos(\omega_l t - I_{spp}\cos(\omega_{sp}t + \varphi) - I_{rp}\cos(\omega_r t)) \quad (12)$$

Input data for the simulation result from (12). Simulation values of I_l, I_{spa}, I_{spp}, I_{ra}, I_{rp}, φ start from the measurement, but various values can also be used. Other data processing is the same as in experiments. Hilbert transform, (9), (10) was used for the IM current amplitude and phase demodulation. The values for a_{APL}, a_{APH} (2nd window in Fig.5) were compared to the values computed from (3),(6). Full identity with the theory was found.

The simulation was also used for the case where angle φ is positive and $a_{APL} < a_{APH}$. But this IM state is not stable and can come only in IM dynamic regime.

Simulation results are depicted in Fig.5. Note that the time course of amplitude demodulated current follows the envelope of IM current – compare the window 3 to the window 1. Time course of amplitude and phase demodulation (windows 3, 4) shows small ripple at the beginning - t=0, given by nonsequenced modulating current in time window.

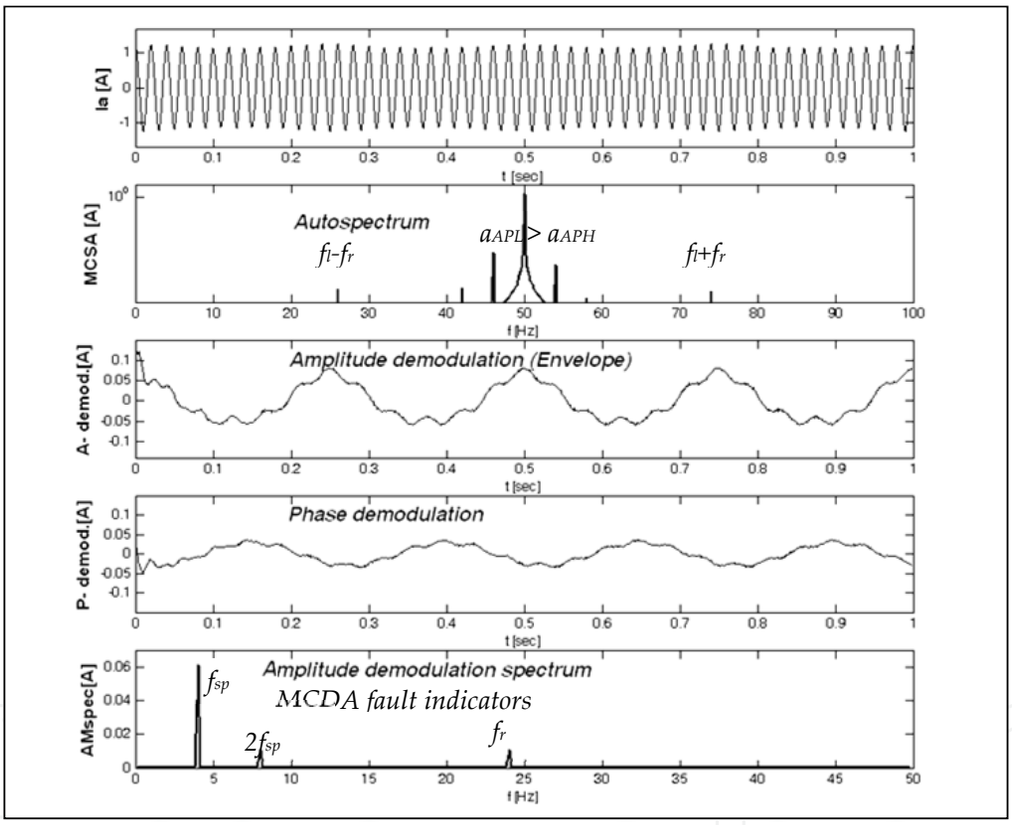

Figure 5. The demodulation analysis of stator current, 4-poles motor 0.75 kW, 2 broken bars, great inertia - φ <0, low dynamic eccentricity. Simulation results.

5. Experimental results

The main aim of the experiments was to verify the introduced theory of JAPM, to verify the both fault indicators I_{spa}, I_{ra} changes at different IM load and to verify the influence of the time varying load.

Two sorts of IM were used for the experiments.

The first IM was SIEMENS type 1LA7083-2AA10, 1.1 kW, two-pole, rated revolutions 2850 min^{-1}, I_{nom}=2.4A, n_{rb} =23, air gap dimension=0.25 mm, health motor, 1 interrupted rotor bar and 2 contiguous interrupted rotor bars, both 3 rotors were balanced with factory set-up dynamic eccentricity (setting the exact value of dynamic eccentricity is at so small air gap very difficult). The 2nd IM was SIEMENS type 1LA 7083-4AA10, 0.75 kW, four-pole motor, I_{nom} = 1.8A, n_{rb} =26, balanced rotor and rotor with 2 contiguous interrupted rotor bars.

Various motors and fault rotors used in experiments were manufactured directly at Siemens Electromotor. Motors were tested at 25%, 50%, 75% and 85% of the full load according to the motor load record from Siemens. The changes in the broken bar fault indicator I_{spa} was also tested in the low load range from no load to 20% of full load.

The experiments were based on Bruel&Kjaer PULSE 20 bits dynamic signal analyzer (DSA) based on the frequency filtration and decimation principle. All channels are sampled simultaneously. FFT analyzer was set on the base band mode, frequency span 100Hz, 400 frequency lines, Δf =0.25Hz, Hanning window, continuous RMS exponential averaging with 75% overlapping. For the experiment of I_{spa} changes at very low load the measuring time T= 32s, Δf =0.03125Hz was used.

To find out the possible differences in both introduced demodulation methods, both Hilbert and space transform were simultaneously evaluated in the real time.

The experiments results were verified by 16 channels PC measurement system based on two 8 channels, 24-bit DSA NI 4472B from National Instruments setting in the lowest possible frequency range 1kHz.

To obtain the maximal measurement accuracy the possible errors in Digital Signal Processing (DSP) should be avoided. Sampling theorem with full agreement between the sampling frequency and surveyed analog frequency band should be strictly kept. At the violation of sampling theorem, signal frequencies higher than Nyquist frequency f_N are tilted - masked to the basic frequency region from $0\text{-}f_N$ and they can create there aliasing frequencies or interfere with regular frequencies, changing their amplitudes. Masking can come through many higher bands of the sampling frequency. Unlike dynamic signal analyzers, simple PC cards and scopes are usually not equipped with anti aliasing filters.

The measurement acquisition time T should be optimally set. Spectral frequency resolution Δf is a reciprocal value of the acquisition window T, $\Delta f = 1/T$.

A great DSP error, both in frequency and magnitude, occurs if the analog frequency of the examined signal is exactly in the centre of Δf. In the case of a rectangular window, the spectral magnitude decline is $sinc(\pi/2)=2/\pi=0.636=-3.92\ dB$, representing 36% fault in magnitude! In the case of Hanning window the decline is $(3/\pi - 1/(3\pi))=0.848=-1.43\ dB$. If the low analog sideband frequency $f_1\text{-}f_{sp}$ is nearer to the discrete spectral frequency than the high sideband frequency f_1+f_{sp}, the a_{APL} can be higher than a_{APH} and vice versa. The optimal acquisition time should be longer than 1sec. e.g. 4sec. with Δf = 0.25Hz. In the case of very low load, the minimal acquisition time 8 sec with Δf = 0.125Hz can be used for the accurate f_{sp} detection and for the decrease of DSP errors probability.

Spectrum averaging, which lowers stator current non-stationary errors, should be always used for the error minimization. FFT computation time is substantially shorter than the acquisition time, so the start of a new acquisition and a new averaging can start earlier than the end of the previous acquisition time. This process is called overlapping. It is expressed in percent of the acquisition time in the range of 0% - no overlapping- to max, when the new acquisition starts immediately at the end of previous FFT. The overlapping implementation (programming) is easy. Overlapping more than 50% is recommended.

Spectrum of demodulated current does not contain any sidebands components, it is transparent and easy readable and only one simple spectral peak is the fault indicator.

The fault indicator I_{spa} [A] for broken bars is the amplitude of the amplitude modulating current on fault frequency f_{sp} so the spectral magnitude of amplitude demodulated IM current on f_{sp}, see Fig.6, 4rd window from the top. The fault indicator I_{ra} [A] for dynamic eccentricity is the amplitude of the amplitude modulating current on fault frequency f_r so the spectral magnitude of amplitude demodulated IM current on f_r, Fig.6, 4rd window.

Fault indicators clearly show the rotor faults but do not show the real fault severity. I_{spa} and I_{ra} amplitudes considerably differ with the IM power.

Fault severity dimensionless coefficients $k_{sp,}$ k_r [%] are fault indicators normalized by a constant value - motor rated current I_{nom}

$$k_{sp} = I_{spa} / I_{nom} \tag{13}$$

$$k_r = I_{ra} / I_{nom} \tag{14}$$

where fault indicators I_{spa}, I_{ra} are expressed in RMS.

In order to keep the independence of fault severity coefficients of the different load, the normalizing value must be a constant. Therefore the coefficients $k_{sp,}$ k_r as the basic evaluating tool for the assessment of fault severity and for the state of rotor bars was suggested.

Five various experiments, presented in paragraphs 5.1 to 5.5, covering different IM states, time varying load and IM energized from inverters were performed.

5.1. The results of MCDA fault indicators for broken bars at different IM load

The complex stator current analysis using simultaneous amplitude and phase demodulation of the two-pole IM is depicted in Fig. 6 – individual windows from above: stator current autospectrum i.e. MCS, AM fault current extracted from the stator current by the amplitude demodulation (9), PM fault current extracted from the stator current by the phase demodulation (10). Corresponding spectra are depicted in the 4th and 5th windows. The time courses of AM and also PM clearly show fault currents with 2 dominating frequencies f_{sp} and f_r which are better seen in the corresponding spectra. It is clearly seen that the phases of AM and PM at f_{sp} are exactly opposite, compare 2nd window to 3rd window from the top.

MCDA fault indicators are depicted in 4th window from the top.

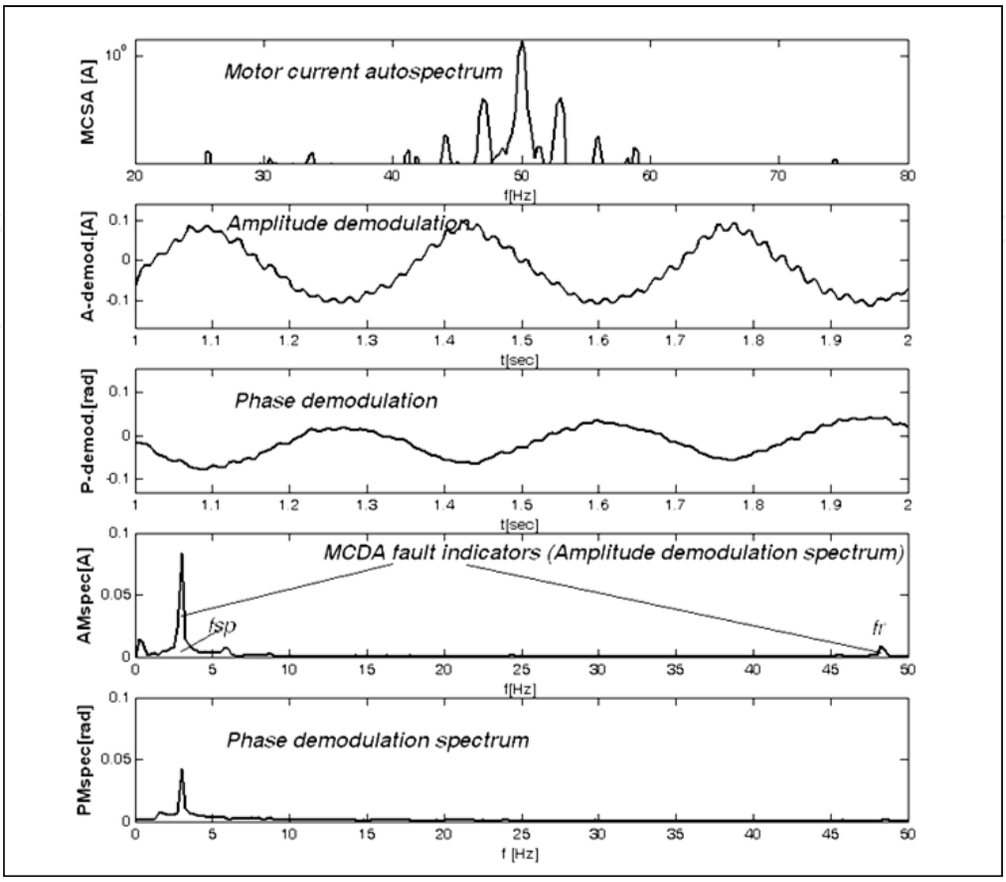

Figure 6. Complex demodulation analysis of IM current, 2-poles 1.1.kW motor, 75% of full load

Demodulation methods suppress large I_l and therefore the relatively accurate linear scale for spectrum can be used, but for the observation of higher harmonics of f_{sp} a logarithmic scale also can be used.

Equation (5) which pays only under steady conditions and low inertia, was verified. The full agreement with the theory of a_{APL} and a_{APH} equality was found in the range of possible a_{APL}, a_{APH} variations, which can be in the range of ± 2.5dB.

There are two reasons for the a_{APL} and a_{APH} variation:

1. The non-stationarity of IM current. The rotor analog current is not a fully stationary signal and therefore the phase shift φ between AM and PM may not be exactly zero and due to small dynamic changes it can oscillate around zero and therefore causes changes in a_{APL} and a_{APH} according to (6). Linear or exponential spectrum averaging lowers this error.
2. DSP errors. DSP errors come owing to the finite Δf which was described in detail in the previous part of this section 5.

The shortened experimental results are briefly summarized in Table 2 (suffix$_H$ for the demodulation using Hilbert transform, suffix$_P$ for the demodulation using space transform) for 2-pole motors and Table 3 for 4-pole motors.

Motor state		25% load	50% load	75% load	85% load
2-poles 1.1.kW	f_r [Hz]	48.95	48.6	48.1	47.6
	f_{sp} [Hz]	1.99	2.8	3.8	4.62
Health motor	I_{spaP} [mA]	9.4	9.5	9.3	8.5
	I_{spaH} [mA]	9.5	9.6	9.6	8.2
	k_{sp} [%]	0.28	0.29	0.28	0.25
1 interrupted rotor bar	I_{spaP} [mA]	35	40	39	39
	I_{spaH} [mA]	36	41	40	39
	k_{sp}[%]	1.11	1.28	1.26	1.25
2 contin. interrupted rotor bars	I_{spaP} [mA]	69	78	79	77
	I_{spaH} [mA]	67	75	77	76
	k_{sp}[%]	1.93	1.98	1.95	2.01
Dynamic ecc. Balanced rotor	I_{raP}[mA]	3.9	3.9	3.9	3.5
	I_{raH}[mA]	3.8	3.9	4.1	3.3
	k_r[%]	0.15	0.15	0.16	0.13

Table 2. Fault Indicators and fault severity coefficients for broken bars and dynamic eccentricity, Hilbert and Space Transforms, 2- poles IM

Motor state		25% load	50% load	75% load	85% load
4- poles 0.75 kW	f_r [Hz]	24.56	24.41	24.21	24.12
	f_{sp} [Hz]	1.73	2.3	3.1	3.45
Health motor	I_{spaP} [mA]	3.3	3.4	3.4	3.3
	I_{spaH} [mA]	3.4	3.3	3.4	3.2
	k_{sp} [%]	0.18	0.18	0.18	0.17
2 contin. interrupted Rotor bars	I_{spaP} [mA]	37	41	43	42
	I_{spaH} [mA]	38	42	43	41
	k_{sp}[%]	1.46	1.68	1.70	1.68
Balanced rotor	I_{raP}[mA]	5.1	5.4	5.3	4.9
	I_{raH}[mA]	5.2	5.5	5.4	4.9
	k_r[%]	0.28	0.28	0.27	0.26

Table 3. Fault Indicators and fault severity coefficients for broken bars and dynamic eccentricity, Hilbert and Space Transforms, 4- poles IM

5.1.1. The experimental results discussion

The experiments proved the correctness of JAPM theory and the correctness of the used demodulation techniques.

The experiments show that broken bar AM is almost insensitive to the motor load. The I_{spa} changes are in the range of 11% within the interval between 25 – 85% and in the range of 7 % in the interval 50 – 85%. The same holds for the fault severity coefficient k_{sp} because the denominator in (13) is a constant value. The values of fault indicator for 2 continuous rotor bars are almost twice greater then indicators for 1 broken bar.

At no load and at low load below 20 % of full load I_{spa} decreases- see Table 5. Therefore for the industrial diagnostics the recommended load range is from 20% of load to the full load. For more accurate diagnostics, the range from 25% of load to the full load is recommended.

Fault severity coefficient k_{sp} for 2 broken bars at 4-poles motor are little smaller in comparison with 2-poles motor owing to a greater number of rotor bars n_{rb} - 26 on 23.

Healthy motor shows some residual modulation, due to irregularities in rotor bars layout, but k_{sp} were not at all measurements greater than 0.3 %.

The acceptable limits for k_{sp}, should be experimentally stated for various motor types because they can differ. Namely the sizes of k_{sp} for large IM can have different acceptable limits.

The values of fault severity coefficient k_r for dynamic eccentricity slightly decrease with increasing load. Over the 85% of full load the decrease is slightly greater. The values of I_{ra} at a factory balanced rotor are still sufficient for a sensorless rotor electromagnetic field speed and speed irregularities measurement (Jaksch & Zalud, 2010). PM for rotor eccentricity slightly decreases with increasing load unlike PM for broken bars.

Two introduced demodulation methods for dynamic rotor fault detection - Hilbert and space transforms - give the same results and both can be used for rotor fault diagnostic. Both measurement systems - Bruel&Kjaer PULSE and NI 4472B give the same fault indicators.

5.2. The comparison of AM and PM at different loads

The second experiment examined the spectral magnitudes of amplitude and phase demodulated IM current on f_{sp} at different loads, together with the comparison of the MCSA low sideband a_{APL} on f_1-f_{sp}. The results are depicted in Fig.7 -9 and summarized in Table 4.

2-poles IM, 1.1 kW 2 broken bars	25% load	50% load	75% load	85% load
AM - MCDA fault indicator I_{spa} [mA]	70	77	78	78
PM [mrad]	24	33	44	49
Low sideband a_{APL} [mA]	36	44	46	48

Table 4. AM and PM, 2 broken bars, at different IM load in comparison to low sideband a_{APL}

The experiment proved the theory that PM substantially increases with increasing load (2nd row in Table 4 and peaks in circles on f_{sp} in lower window in Fig.7 to Fig.9).

PM increases 2.2 times within the interval between 25 - 85%. The increase of PM spectral magnitude a_P is caused both by I_1 increase at increasing load and also by I_{spp} increase, (3). It is the real cause of MCS fault indicators a_{APL} and a_{APH} increasing with increasing load, Fig.3 and (5).

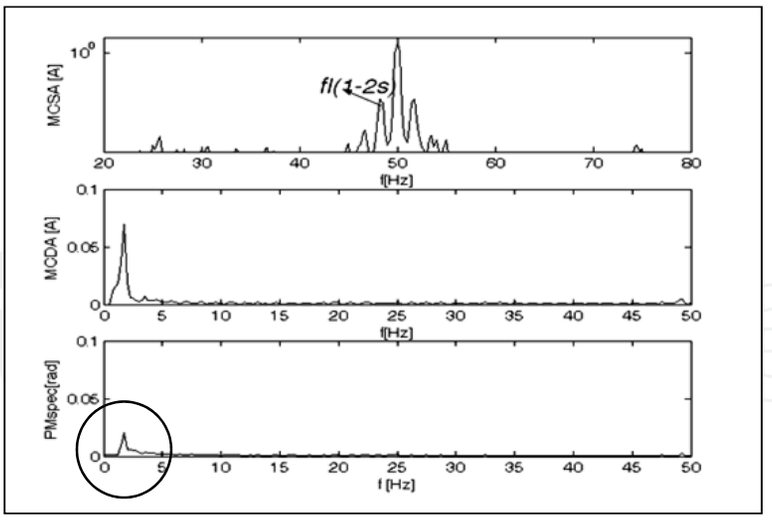

Figure 7. IM spectrum, spectrum of amplitude and phase demodulated current, 25% of full load

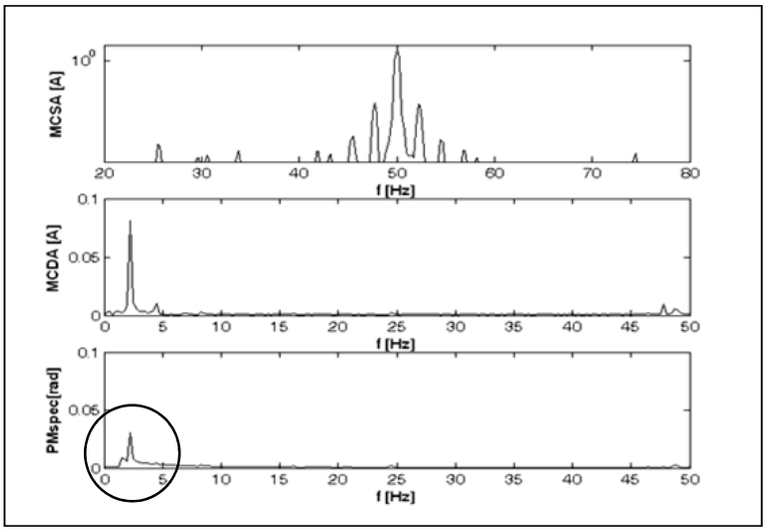

Figure 8. IM spectrum, spectrum of amplitude and phase demodulated current, 50% of full load

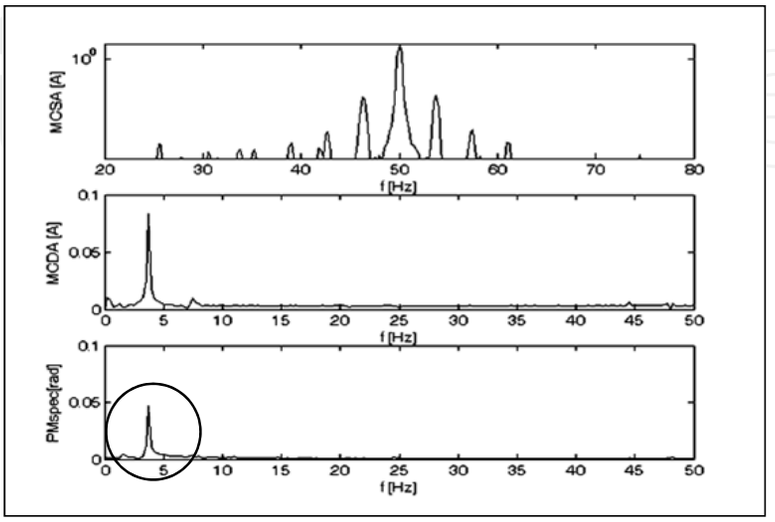

Figure 9. IM spectrum, spectrum of amplitude and phase demodulated current, 85% of full load

5.3. The analysis of indicator I_{spa} at very low load from no load to 20 % of full load

The 3rd experiment analyses the changes of I_{spa} in the range of no load to 20 % of full load. Table 5 shows the MCDA broken bars fault indicator I_{spa} decline under 20% of full load. For very low load at s=0.44%, f_{sp}=0.44 Hz the I_{spa} for 2 broken bars decreases to I_{spa}=31mA, which is approximately the half of its nominal value and it corresponds to I_{spa} for 1 broken bar (Table 2), so great confusion in broken bar diagnostics may come.

s[%]	0.21	0.37	0.44	0.69	0.94	1.16	1.37
f_{sp} [Hz]	0.21	0.37	0.44	0.69	0.94	1.16	1.37
I_{spaH} [mA]	19	25	31	37	47	56	69

Table 5. I_{spa} changes from no load to 20% of full load, 2 broken bars, 1.1.kW IM

The decrease of I_{spp} representing PM, and therefore the decrease of MCSA fault indicators a_{APL}, a_{APH} under 20% are substantially faster than the decrease of MCDA fault indicator I_{spa} (Fig.7–Fig.9, PM in circles).

5.4. IM rotor fault diagnostics at time varying load

The aim of 4th experiment was to verify presented theory of the time varying load and its influence on MCDA fault indicator I_{spa}. The time varying load frequency f_{load} = 4 Hz was chosen very near to the broken bars fault indicator frequency f_{sp} =1.9 Hz.

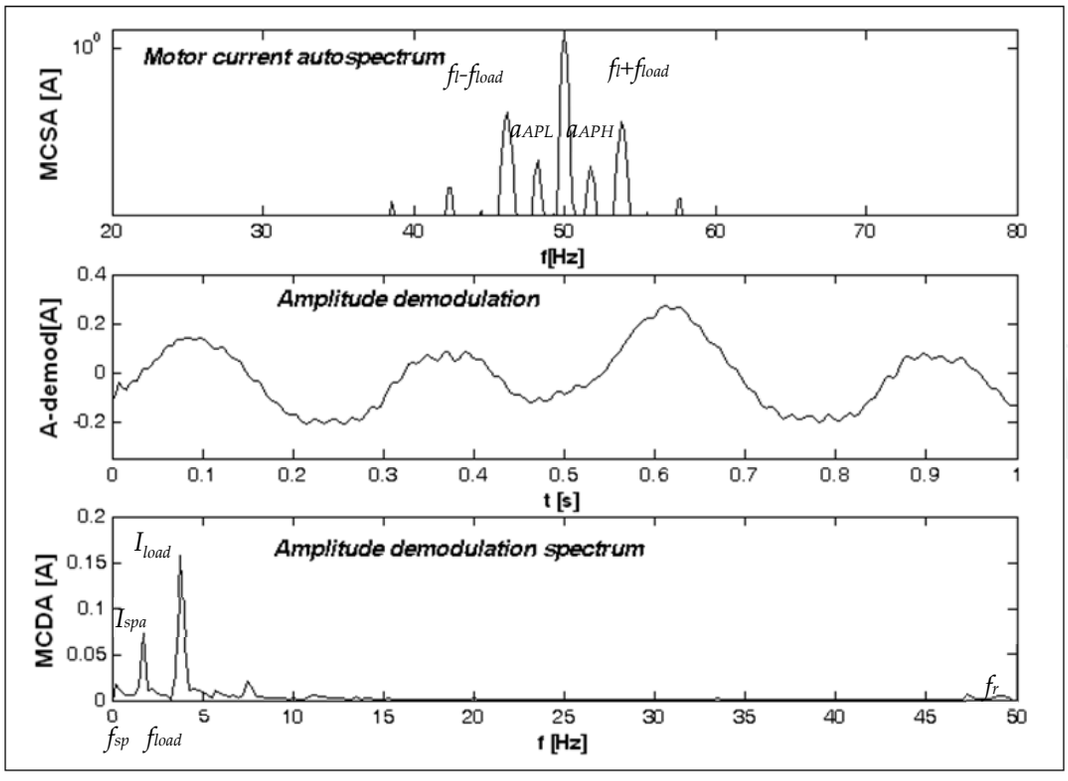

Figure 10. Windows from above: MCS, time course of amplitude demodulated current, and its MCDA spectrum, 25% of full load.

Experimental results are depicted in Fig.10. Additional two new spectral sidebands appear on frequencies $f_l \pm f_{load}$ in MCSA spectrum-upper window and one new spectral peak appears on f_{load} in MCDA spectrum –lower window.

The time course of amplitude demodulated current, so the time course of amplitude modulating (i.e. fault) current is depicted in the middle window. The sum of three harmonic with the fundamental amplitudes I_{spa}, I_{load} and I_r and corresponding frequencies f_{sp}, f_{load} and small ripple from f_r is clearly visible.

The broken bar fault indicator I_{spa} did not change its amplitude (compare with Fig.7). The important conclusion is that the size of MCDA fault indicator I_{spa} is not influenced by the time varying load.

5.5. IM energized from inverters

The last experiment examined two-pole IM with 2 broken bars energized from inverters. Two PWM open-loop inverters were used. The measurements were made at low inertia and at a stable motor load.

In the first measurement, an inverter was properly rated. In this case, the results correspond to the results for IMs energized from line. The MCS $a_{APL} = a_{APH}$ and time course of AM and PM was completely opposite.

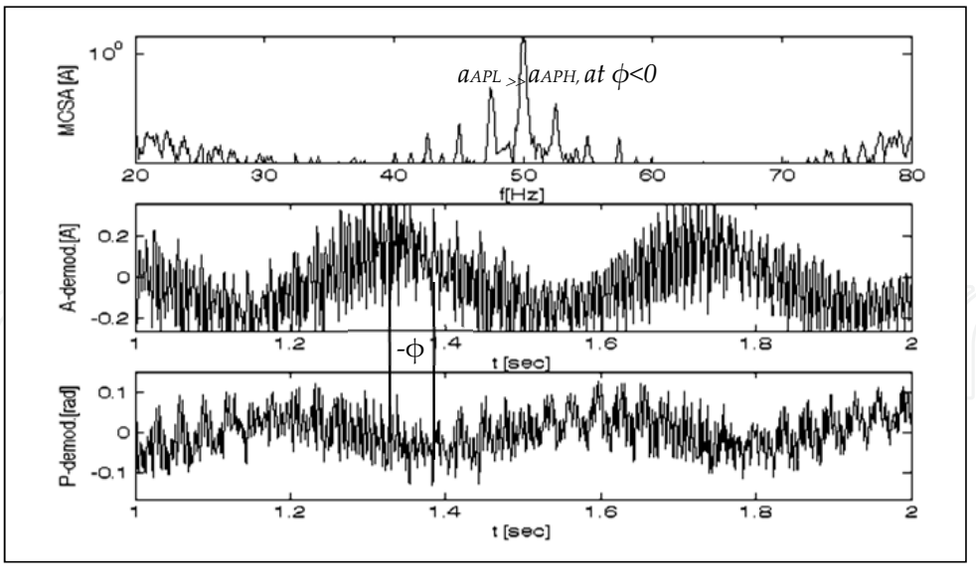

Figure 11. Inverter fed IM, low DC-link and overloaded, low inertia, 75% of full load, MCS, time course of amplitude and phase demodulated current, PM delays -φ behind AM.

In the second measurement another inverter was not properly rated and its DC-link voltage was only 400V. IM was fed by lower voltage apps. 185V and therefore was overloaded. In

this case the MCS $a_{APL} > a_{APH}$ appeared (the same phenomenon which can appear at great inertia). The demodulation detected PM delay $-\varphi$ behind AM -see Fig.11 and validated the explanation of $a_{APL} > a_{APH}$ in Fig.4., and also the correctness of (6).

This phenomenon of PM delay behind AM at low inertia appears when an AC source is not properly dimensioned, its feeding voltage is lower than nominal voltage and therefore it is not able to fully excite IM.

It can be concluded that continual increasing of a_{APL} above a_{APH} (out of the range of possible a_{APL} and a_{APH} variations± 2.5dB) generally means, that IM working conditions are out of the normal.

6. Demodulation analysis versus direct analysis

The presented MCDA and following AM and PM synthesis to the full IM current fault indicators a_{APL}, a_{APH} (6) enables the comparison of the demodulation analysis to the direct full IM current analysis.

The IM stator current demodulation analysis enables to find out the complex changes in the rotor electromagnetic field and MMF. Based on this analysis the new method MCDA was introduced. MCDA comes from the basic fundamental which occurs at dynamic rotor faults – JAPM. MCDA senses the whole stator current, but before the further evaluation as spectral analysis, it extracts time courses of fault currents directly induced by dynamic rotor faults. Anything more accurate than the extraction and direct processing of fault currents cannot exist.

The phase demodulation extracts PM current and can be used for the research of rotor magnetic field changes and oscillation and for the sensorless speed measurement. PM is not very suitable for rotor fault diagnostics, because the fault indicators are dependent on motor load.

The amplitude demodulation extracts AM fault current. AM is from 20% of full load almost independent of motor load and it is the base for rotor fault diagnostics not dependent on different load and inertia. Broken bar and dynamic eccentricity fault indicators are simple spectral peaks at direct fault frequencies f_{sp}, f_r (no sidebands). The amplitude demodulation can be easily implemented continually in a real time.

MCDA is a clear, very simple and reliable method and it is very useful for industrial application both for diagnostics and also for IM continual monitoring.

Methods of the direct analysis of IM current sense and subsequently process the full IM current. The great disadvantage of the direct IM current analysis is that its fault indicators a_{APL}, a_{APH} are dependent on IM load and inertia moment. The second disadvantage is that fault frequencies cannot be determined directly, but as a difference from f_1, which can change. The third disadvantage is the lower resolution both in frequency and amplitude.

Great differences between the magnitudes of the main spectral peak on f_l and the sidebands magnitudes a_{APL}, a_{APH} requires the use of logarithmic or dB scale.

The presented demodulation analysis of IM current proved that IM current at dynamic rotor faults is not so simple and inwardly contains JAPM. Simply to say stator current consists of 3 parts - stator current of health motor, amplitude modulating current and phase modulating current (12). Just JAPM is the main reason for of the full current based fault indicators dependences on motor load and inertia.

The demodulation analysis exactly established the reasons for a_{APL} and a_{APH} formation and developed equations for their computation (5), (6). Consequently the MCDA has allowed a complete explanation of both MCS load and inertia dependences: MCS fault indicators a_{APL}, a_{APH} actually consist of 3 variables - AM, PM and φ, (6). PM increases with the increasing load (Fig.7-9, Table 4) and therefore causes the increase of both a_{APL} and a_{APH}. Great inertia or poorly fed IM causes that the angle φ changes from zero values to negative values and therefore $a_{APL} > a_{APH}$ (6). The summation or averaging of a_{APL} and a_{APH} is inaccurate, because the equation (6) is not a linear function.

The processing and direct analysis of the whole stator current does not enable the distinction of the individual AM, PM and φ contribution to the a_{APL} and a_{APH} and the result is the continual dependence of MCSA a_{APL} and a_{APH} fault indicators on IM load and inertia. No improvements and sophistication of the measurement and evaluation methods can reduce this dependence. Logarithmic or dB scale has to be used for a_{APL} and a_{APH} displaying. It together means the low resolution both in amplitudes and frequencies.

7. Conclusion

Dynamic rotor faults cause dynamic changes of rotor electromagnetic field and MMF and therefore the motor current AM and PM together creating JAPM.

Based on this theory, the new diagnostic method MCDA was developed. Basic properties of AM and PM at rotor faults were presented. The analyses of IM current and current signature at rotor faults together with mathematical equations for low and high autospectral magnitudes computation were derived. These equations were verified by simulation and experimentally and the possible low and high autospectral magnitudes variation due to IM current nonstationarity and DSP errors were discussed.

Two demodulation methods based on Hilbert transform and space transform are presented. Space transform gives the same results as Hilbert transform.

The phase demodulation extracts the fault PM current. PM can be used for the research of rotor magnetic field phase changes and oscillation and for the sensorless rotor magnetic field speed measurement. PM fault indicators are dependent on the motor load.

The amplitude demodulation extracts the fault AM current. The simple spectral peaks at fault frequencies f_{sp} and f_r are the dynamic rotor faults indicators almost independent on IM

load and inertia. It was also proved that MCDA fault indicators are not influenced by the time varying load.

The presented diagnostic method is very clear and can be easily used for a reliable rotor faults diagnostics in a real time or for continual IM monitoring.

Author details

Ivan Jaksch
Technical university of Liberec, Czech Republic

Acknowledgement

The author gratefully acknowledges the contributions of the Grant Agency of Czech Republic.

Appendix

Nomenclature

AM	Amplitude Modulation
PM	Phase Modulation
JAPM	Joint Amplitude Phase Modulation
MCDA	Motor Current Demodulation Analysis
MCS	Motor Current Signature -a_{APL}, a_{APH}
IM	Induction motor
a_{AL}, a_{AH}	Low and high spectral magnitudes of AM
a_{PL}, a_{PH}	Low and high spectral magnitudes of PM
a_{APL}, a_{APH}	Low and high spec. mag. of MCS at JAPM –real motor state
f_{sp}	Slip pole frequency – $2sf_l$
f_r	Motor rotation frequency
f_l	Motor supply frequency
f_{load}	Time varying load frequency
$f_{L,H}$	Low and high spectral sidebands frequencies
$H(t)$	Analytical signal created by Hilbert transform
I_l	Induction motor current amplitude
I_{nom}	Induction motor nominal current amplitude
$i_d(t)$, $i_q(t)$	Real and imaginary part of space vector
I_{spa}	AM current amplitude at f_{sp} frequency, **broken bars fault indicator**
I_{spp}	PM current amplitude at f_{sp} frequency

$\boldsymbol{I_{ra}}$	AM current amplitude at f_r frequency, dynamic eccentricity fault indicator
I_{rp}	PM current amplitude at f_r frequency
I_{load}	AM current amplitude at f_{load} frequency,
$J_i(I_{spp})$	i^{th}-order Bessel function of the first kind
$k_{sp,}$	Fault severity coefficient for broken bars
k_r	Fault severity coefficient for dynamic eccentricity
$magH(t)$	Absolute value of the complex analytical signal
n_{rb}	Number of rotor bars
p	Number of motor poles
$P(t)$	Analytical signal from the space vector
s	Per unit slip
$\beta(t)$	Phase of the complex analytical signal
φ	Phase angle of PM in reference to AM at broken bars

8. References

Bellini, A., Filippeti, F., Tassoni, C. & Kliman, G.B. (2001). Quantitative evaluation of induction motor broken bars by means of electrical signature analysis. *IEEE Transactions on industry applications,* vol. 37 pp. *1248-1255.*

Bellini, A., Filippetti, F., Tassoni, C. & Capolino, G.-A. (2008) Advances in Diagnostic Techniques for Induction Machines, *IEEE Trans. on Industrial. Electronics,* vol. 55, pp 4109-4126.

Bendat, J.S. (1989). *The Hilbert Transform*, Bruel &Kjaer Publication BT0008-11, DK 2850, Naerum, Denmark.

Blödt, M., Bonacci, D., Regnier, J., Chabert, M. & Faucher, J. (2008). On-line monitoring of mechanical faults in variable-speed induction motor drives using Wigner distribution, *IEEE Transactions on Industrial Electronics.,* vol. 55, no. 2, pp. 522–533

Concari, C., Franceschini, G. & Tassoni, C. (2008). Differential Diagnosis Based on Multivariable Monitoring to Assess Induction Machine Rotor Conditions, *IEEE Transactions on Industrial Electronics,* vol. 55, no. 12, pp. 4156-4166.

Cusido, J., Romeral, J.A., Ortega, J.A., Rosero, A. & Garcia Espinosa A. (2008). Fault Detection in Induction Machines Using Power Spectral Density in Wavelet Decomposition, *IEEE Transactions on Industrial Electronics,vol.55,* no.2, pp.633-643

Dorrell, D. G., Thomson, W. T. & Roach, S. (1997). Analysis of airgap flux, current, and vibration signals as a function of the combination of static and dynamic airgap eccentricity in 3-phase induction motors, *IEEE Transactions on Industrial Application.,* vol. 33, no. 1, pp. 24–34.

Drif, M. & Cardoso, A.J.M. (2008). Airgap-Eccentricity Fault Diagnosis, in Three-Phase Induction Motors, by the Complex Apparent Power Signature Analysis, *IEEE Trans. on Industrial Electronics,* vol. 55, no. 3, pp. 1404-1410, March 2008.

Jaksch, I. (2003). Faults diagnosis of three-phase induction motors using envelope analysis, *Proceedings of 4th IEEE International Symposium on Diagnostics for Electric Machines, Power Electronics and Drives,* ISBN 0-7803-7838-5, pp. 289–295, Atlanta, USA, 9/2003

Jaksch, I. & Zalud, J. (2010). Rotor Fault Detection of Induction Motors by Sensorless Irregularity Revolution Analysis, *Proceedings of XIX International Conference on Electric Machines,* ISBN 978-1-4244-4175-4, Paper number RF-001511, Rome, 9/2010.

Joksimovic, G. M. (2005) Dynamic simulation of cage induction machine with air gap eccentricity, *Proceedings of Institute. Elect. Eng.—Electric Power Appl*., vol. 152, no. 4, pp. 803–811.

Jung, J.H., Lee, J.J. &. Kwon B. H. (2006). Online Diagnosis of Induction Motors Using MCSA. *Transactions on Industrial Electronics*, vol.53, no.6, pp.1842-1852..

Kia, S.H., Henao, H. & Capolino, G.-A. (2009). Diagnosis of broken bar fault in induction machines using discrete wavelet transform without slip estimation, *IEEE Transactions on Industry Applications,* vol. 45, no. 4, pp. 1395-1404.

Kia, S.H.; Henao, H.& Capolino, G. (2010). Torsional vibration Assesment Using Induction Machine Electromagnetic Torque Oscillation, *IEEE Trans. on Ind. electronics*, vol. 57, pp. 209-219.

Kral, C., Pirker, F., Pascoli, G. & Kapeller, H. (2008). Robust Rotor Fault Detection by Means of the Vienna Monitoring Method and a Parameter Tracking Technique, *IEEE Transactions on industrial electronics,* vol. 55, pp. 4229-4237

Lebaroud, G. & Clerc, A. (2008). Classification of Induction Machine Faults by Optimal Time–Frequency Representations, *IEEE Trans. on Industrial Electronics*, vol. 55, no. 12, pp. 4290-4298.

Mirafzal,B. & Demerdash, N. (2005). Effects of Load Magnitude on Diagnosing Broken Bar Faults in Induction Motors Using the Pendulous Oscillation of the Rotor Magnetic Field Orientation, *IEEE Transactions on industry applications*, vol. 41, pp. 771-783.

Nandi, S., Toliyat, H. A. & Li, X. (2005). Condition monitoring and fault diagnosis of electrical motors - A review, *IEEE Transactions on Energy Conversion*., vol. 20, no. 4, pp. 719–729.

Randall, R.B. (1987). *Frequency analysis*, Bruel&Kjaer Publication, ISBN 87 8735 14 0

Riera-Guasp, M., Antonino-Daviu J. A., Roger-Folch J. & Molina Palomares, M. P. (2008). The use of the wavelet approximation signal as a tool for the diagnosis of rotor bar failures, *IEEE Trans. Industrial Appl*., vol. 44, no. 3, pp. 716–726.

Su, H. &. Chong, K. T. (2007). Induction machine condition monitoring using neural network modeling, *IEEE Transactions on Ind. Electronics,* vol. 54, no. 1, pp. 241–249.

Thomson, W. & Fenger, M. (2001). Current signature analysis to detect induction motor faults. *IEEE Industry Application Magazine.*, vol. 7, no. 4, pp. 26–34.

Zhang, P, Du, Y., Habetler, T. G. & Lu B. (2011). A Survey of Condition Monitoring and Protection Methods for Medium-Voltage Induction Motors, *Transactions on Industry application,* vol.47, pp.34-46

Zidani, F., Diallo, D., Benbouzid, M.E.H. & Nait-Said, R. (2008). A Fuzzy-Based Approach for the Diagnosis of Fault Modes in a Voltage-Fed PWM Inverter Induction Motor Drive, , *IEEE Transactions on Industrial Electronics*, vol.55, no.2, pp.586-593

IntechOpen